Mechanochemical design of hemoglobin-functionalised magnetic nanomaterials as energy storage devices

Daily Rodríguez-Padrón[a], Alain R. Puente-Santiago[b], Alvaro Caballero[c], Almudena Benítez[c], Alina M. Balu[a], Antonio A. Romero, Rafael Luque[a]*

[a]*Departamento de Química Orgánica, Grupo FQM-383, Universidad de Cordoba, Campus de Rabanales, Edificio Marie Curie (C-3), Ctra Nnal IV-A, Km 396, E14014, Cordoba (Spain), e-mail: g62alsor@uco.es*

[b]*Departamento de Química Física, Universidad de Cordoba, Campus de Rabanales, Edificio Marie Curie (C-3), Ctra Nnal IV-A, Km 396, E14014, Cordoba*

[c]*Departamento de Química Inorgánica e Ingeniería Química, Campus de Rabanales, Edificio Marie Curie (C-3), Ctra Nnal IV-A, Km 396, E14014, Cordoba*

Abstract

A bio-modified nanomaterial based on horse hemoglobin (Hb) and cobalt oxide magnetic nanoparticles (Co_3O_4 MNPs) was synthesized using a simple solventless mechanochemical dry milling step. Dopamine (DA) was employed as a robust scaffold to design the stable nanostructures. The nitrogen band (400 eV) in the XPS spectrum, together with zeta potential measurements support the presence of Hb in the obtained nanostructure. Additionally, the amide I and amide II bands at 1654 cm^{-1} and 1545 cm^{-1} in the FT-IR spectrum suggest that Hb does not undergo changes in its secondary structure. This assumption was also confirmed by Resonance Raman spectroscopy. TEM images reveals a homogeneous distribution of the Hb-DA-Co_3O_4, with a particle diameter of 10.1±0.2 nm. Functionalised materials exhibited a relevant magnetism, preserved upon functionalisation. The functionalised Hb-DA-Co_3O_4 nanocomposite was successfully employed in the design of a

supercapacitor (specific capacitance average: 115 Fg^{-1}) with excellent cycling durability, over 94% specific capacitance retained after 1000 cycles.

Introduction

Bio-modified magnetic nanoparticles have attracted significant attention in the past decade.[1-3] A wide range of novel nanomaterials have been designed taking advantage of the unique properties of magnetic nanoparticles, which can be easily manipulated and separated from the bulk solution by a magnetic field gradient. This behaviour opened exciting opportunities in many areas of biotechnology, biosensing and biomedicine such as enzyme immobilization,[4, 5] nucleic acid detachment,[6, 7] protein adsorption and purification,[8, 9] cell sorting[10, 11] and drug delivery.[12, 13]

Various strategies have been developed to functionalize biological molecules on magnetic nanoparticle surfaces. One successful strategy involves the covalent binding of small molecules to MNPs surfaces to provide specific functional groups that can favour further coordination of biomolecules including DNA, antibodies, enzymes and proteins.[14] Dopamine (was frequently employed as a versatile and robust scaffold to immobilize biomolecules on MNPs[15, 16] due to the good stability of the resulting nanostructures, simplicity in linkages and the ability to restructure under-coordinated Fe surface sites back to a bulk-like lattice structure with an octahedral geometry for oxygen-coordinated iron.[17] Nevertheless, nearly all reported synthetic methods have been conducted in aqueous phase and/or solution with inherent drawbacks including negative solvent effects and lack of control over surface chemistry.

In order to simplify the synthesis of bio-modified magnetic nanoparticles, reducing both reaction times and circumventing solvent issues, mechanochemical processes offers a valuable alternative to traditional routes.[18] This simple, inexpensive, reproducible and greener methodology has been demonstrated to be highly useful for

the design of a range of advanced nanomaterials.[19-21] Interestingly, mechanochemistry has not been reported to date for the preparation of bio-conjugates based on proteins and magnetic nanoparticles.

In this regard, Hemoglobin (Hb) is an excellent candidate to be used in mechanochemical synthesis due to its robustness, commercial availability, moderate cost and known well documented structure.[22] This protein possesses a quaternary structure that contains four polypeptide chains (globin chains) and one heme group bound to each of the globin chains which can store and transport oxygen in muscle cells in vertebrate animals.[23]

Metalloproteins such as c-type cytochrome immersed in an electrically conductive matrix of microbial biofilms has been proven to act as pseudo-capacitors.[24] The redox groups of the cytochrome give rise to fast surface redox reactions[25] which can provide high electron storage capacity and high specific capacitances to the biofilm. These preliminary results opened innovative possibilities for capacitors design which have attracted interest in energy storage since supercapacitors have the potential to complement or replace batteries.

Inspired by such an original approach, our research group proposes herein the first mechanochemical strategy that combines magnetic nanomaterials with proteins towards the design of a novel bio-inspired supercapacitor under dry milling using dopamine as a robust linker. The concept of the proposed methodology is depicted in Scheme 1.

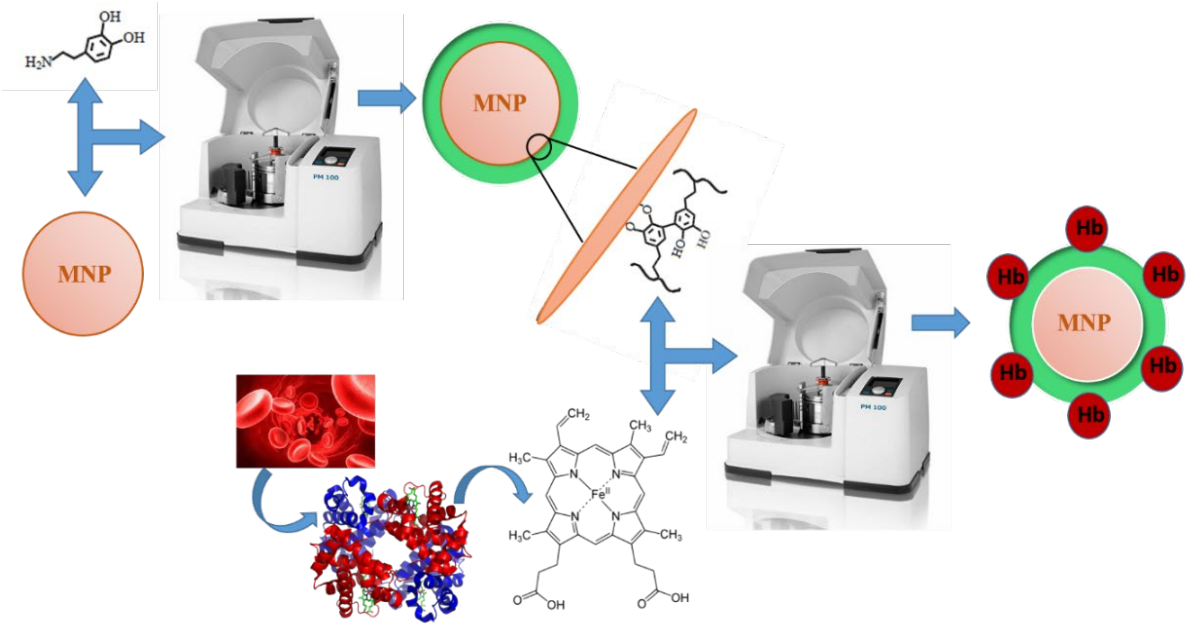

Scheme 1 Overview of the preparation of the Hb-DA-Co_3O_4 bio-modified material

Experimental part

Synthesis of bio-modified magnetic nanoparticles: Hb-DA-Co_3O_4

Horse hemoglobin (Hb) and dopamine hydrochloride (DA-HCl), together with pre-synthesized Co_3O_4 magnetic nanoparticles (MNPs) were utilised to develop a new bio-modified nanomaterial by mechanochemical milling processes. In a first step, 125 mg of DA-HCl was solved in 600 µL of ultrapure water and added to 500 mg of MNPs. This mixture was milled in a Retsch PM100 ball mill under typical optimized conditions from previous work of the group (i.e. 200 rpm, 10 min),[26] resulting in DA-Co_3O_4. The synthesis of Hb-DA-Co_3O_4 was subsequently conducted by milling a dispersion of 100 mg of Hb in 600 µL of NaH_2PO_4 buffer (pH=7) together with DA-Co_3O_4 under identical grinding conditions. Hb-DA-Co_3O_4 obtained after milling was washed five times with ultrapure water to remove any weakly physisorbed protein and finally oven dried at 30ºC for 24h.

Material Characterization

Hb-DA-Co_3O_4 bio-modified material was characterized by X-ray Photoelectronic Spectroscopy (XPS), Transmission Electronic Microscopy (TEM), Dynamic Light Scattering (DLS), Fourier Transform-Infrared Spectroscopy (FT-IR) and Raman spectroscopy, in order to prove the protein immobilization on MNPs.

The X-ray diffraction patterns of both, Co_3O_4 MNPs and Hb-DA-Co_3O_4 bioconjugate were collected using the D8 Advanced Diffractometer (Bruker AXS) with the Lynxeye detector, at room temperature. The 2θ scan range was from 10° to 70°, with a step size of 0.02° and a counting time of 0.2 second for phase identification and 1 second for phase quantification. Phase identifications were conducted using the Bruker Diffrac-plus EVA software, supported by the Powder Diffraction File (PDF) database of the International Centre for Diffraction Data (ICDD).

XPS analysis was conducted at the Central Service of Research Support (SCAI) of the University of Cordoba, using an ultrahigh vacuum (UHV) multipurpose surface analysis system SpecsTM. The experiment was carried out at pressures $<10^{-10}$ mbar, using a conventional X-ray source (XR-50, Specs, Mg-Kα, hv=1253.6 eV, 1 eV = 1.603 x 10^{-19} J) in a "stop and go" mode. The sample was deposited on a sample holder using a double-sided adhesive tape, and afterwards evacuated overnight under vacuum ($<10^{-6}$ Torr). Spectra were collected at room temperature (pass energy: 25 and 10 eV, step size: 1 and 0.1 eV, respectively) with the Phoibos 150-MCD energy detector. The XPS CASA program was employed for deconvolution of the obtained curves.

FTIR spectra were recorded on an infrared spectrophotometer (ABB MB3000 with Horizon MBTM software), equipped with an ATR PIKE MIRacleTM sampler, a window of ZnSe, and 256 scans at a resolution of 8 cm^{-1}. During the measurements the sample was purged with a dehydrated and deoxygenated nitrogen flow (20 mL min^{-1}). Spectra were recorded at

room temperature in a 4000-600 cm^{-1} wavenumber range. UV-visible absorption spectra were performed on the Jasco UV-visible-NIR (model V-570) spectrophotometer.

Raman measurements were carried out on a XploRA PLUS Raman spectrometer with a 532 nm excitation laser, a standard spectral resolution of 8 cm^{-1}, and a step mapping stage of 0.1 μm with SWIFT™ imaging. The LabSpec Spectroscopy Suite software was used to obtain the spectra.

TEM analysis was performed in the FEI Tecnai G^2 system, equipped with a CCD ("charge coupling device") camera. The sample was dispersed in ethanol and directly deposited on a copper grid, previous to analysis.

The particle size distributions and zeta potential of DA-Co_3O_4 and Hb-DA-Co_3O_4 bioconjugate were analyzed using Zetasizer Nano ZSP (Malvern Instruments Ltd.,UK) instrument. The samples were previously diluted in 10 mM of KNO_3 and the measurements were recorded in triplicate (n = 3) at 25 °C.

Thermogravimetric analysis was accomplished by simultaneous TG-DTA measurements using a Setaram Setsys 12 TGA thermobalance. Samples were heated at a rate of 10 °C min^{-1} under nitrogen atmosphere (40 mL min^{-1}) in the 50–1000 °C temperature range.

The magnetic susceptibility of both Hb-DA-Co_3O_4 and Co_3O_4 materials was evaluated at room temperature and at low frequency (470 Hz), employing a Bartington MS-2 instrument.

Electrochemical experiments

Cyclic voltammetry (CV) measurements were performed in a Potenciostat/Galvanostat Autolab (Solartron1286), 5 sequential cycles were programmed at scan rates of 100 mV/s in a potential window of -0.5–0.7 V. A two-electrode configuration consisting of Hb-DA-Co_3O_4 nanocomposite as working electrode and a Pt foil as counter electrode was used.

The charging/discharging measurement was carried out through chronopotentiometry analysis (CP) at a scan rate of 30 Ag^{-1} in a voltage range of 0-0.8 V using a multichannel potentiostat–galvanostat system (Arbin BT2000). The specific capacitance of the Hb-DA-Co_3O_4 electrodes was calculated from the galvanostatic discharging curves by:

$$C_m = \frac{I \cdot \Delta t}{\Delta E \cdot m} \quad \text{(equation 1)}$$

where C_m is the specific capacitance of the supercapacitor, I is the current of the charge–discharge, ΔE is the potential range, Δt is the discharging time period in seconds, and the m is the mass load of active materials.

Results and discussion

Hb-DA-Co_3O_4 bio-modified nanomaterial was characterized using several techniques including magnetic susceptibility measurements. The structure and arrangement of the Hb-DA-Co_3O_4 and Co_3O_4 nanomaterials has been investigated by X-ray Diffraction measurements. The diffraction peaks of both samples can be indexed to the spinel Co_3O_4 phase, with the appearance of an amorphous phase after the functionalization (see Fig. S1, ESI†).

A comparison between Hb-DA-Co_3O_4, DA-Co_3O_4 and the parent Co_3O_4 MNPs by X-ray photoelectron spectroscopy indicated the presence of Co^{3+} species in the three materials from the Co2p peak around 788.0 eV. Importantly, the presence of nitrogen (N1s~401.0 eV) on the surface of Hb-DA-Co_3O_4 and DA-Co_3O_4 was clearly visualised in the survey XPS spectrum (see Fig. 1a and S2 and S3, ESI†), which was absent in MNPs. Fig. 1c shows two peaks at 400.1 and 402.4 eV in the Hb-DA-Co_3O_4 spectrum, which can be attributed to the N from amino groups and N in the porphyrinic groups of the protein, respectively.[27] This is a clear indication of the presence of the protein on the surface of the MNPs after mechanochemical functionalisation. Additional bands corresponding to C1s (285.0 eV) and

O1s (531.9 eV) also appear in the spectra of the materials, being evidently higher for Hb-DA-Co_3O_4. Specifically, the deconvoluted high-resolution XPS spectrum of C 1s (Fig. 1b) exhibited three different contribution at 284.6, 286.1 and 288.0 eV, associated to C-C/C=C, C-N and C-O from the protein chain, respectively. These findings further supported the presence of Hb in the obtained bio-conjugated nanostructure.

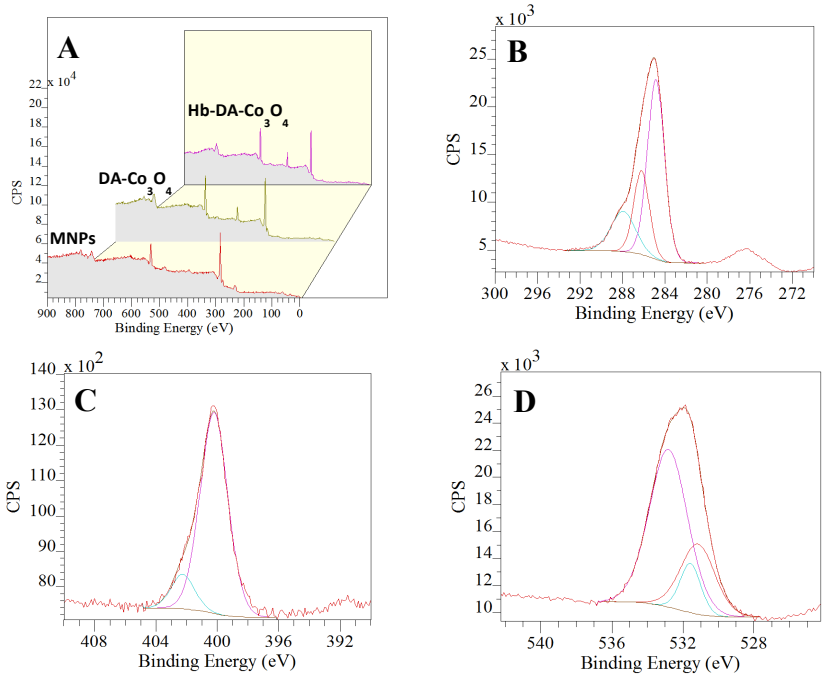

Fig. 1 (a) XPS survey of Hb-DA-Co_3O_4, DA-Co_3O_4 and Co_3O_4 MNPs. Deconvoluted high-resolution XPS spectra of Hb-DA-Co_3O_4 for (b) C 1s, (c) N 1s and (d) O 1s.

The conformation of immobilized Hb on the surface of MNPs was examined by FT-IR. The successful functionalisation of the surface could be confirmed by the presence of amide I and amide II bands from Hb at 1654 cm^{-1} and 1545 cm^{-1}, respectively (Fig. 2.A). The former band (1700–1600 cm^{-1}) can be attributed to the C=O stretching vibration of peptide linkages in the backbone of the protein, while the latter (1620–1500 cm^{-1}) results from the combination of N-H bending and C–N stretching. Amide I and II bands observed in the spectra of Hb-DA-Co_3O_4 are substantially at the same wavelength of those obtained for Hb in solution (1650 cm^{-1} and 1540 cm^{-1}), suggesting that Hb does not undergo any structural changes in its secondary structure, with a preserved native-like structure after the mechanochemical milling process, as expected due to the mild milling conditions (200 rpm, 10 min). Functionalisation experiments run at longer milling times (30 mins) do not seem to induce changes in the protein structure. This hypothesis was also corroborated by UV-vis measurements. Additionally, the UV-vis spectrum of DA-Co_3O_4 was also obtained (see Fig. S4, ESI†).

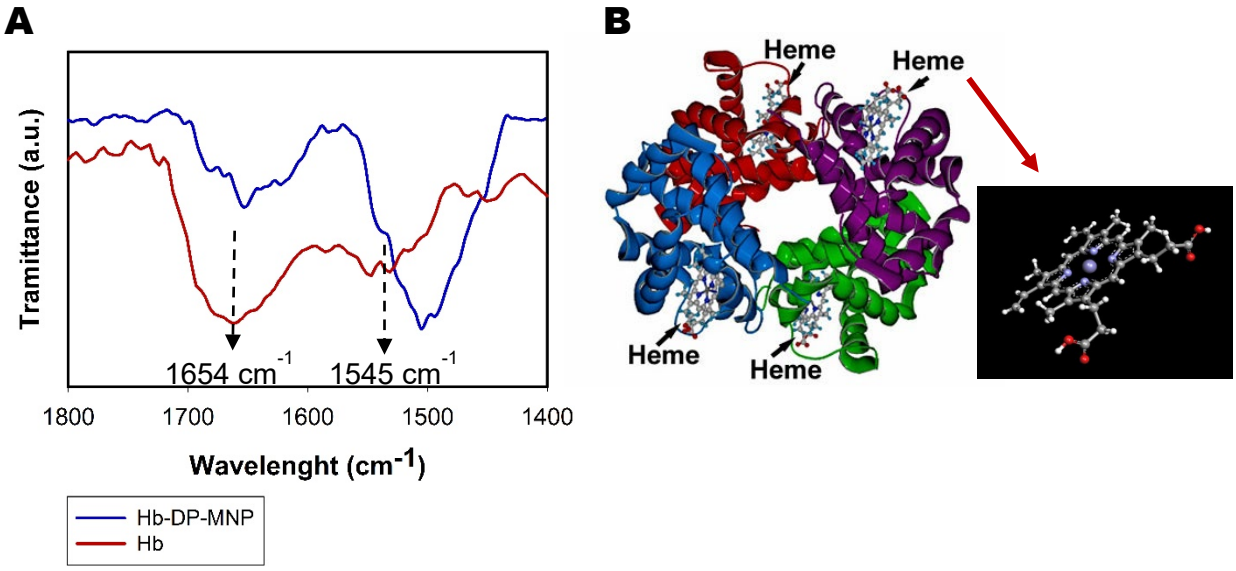

Fig. 2 (A) FT-IR spectra of the Hb-DA-Co_3O_4 and Hb; (B) structure of horse hemoglobin

Fig. 3 displays a representative RR spectrum of the hybrid nanomaterial at 532 nm. Four prominent peaks located at 476, 515, 614 and 684 cm^{-1} can be observed, which correspond

to E_g, $F_{2g}^{(2)}$,$F_{2g}^{(1)}$ and O_h^7 Raman active modes of the inorganic core formed by the spinel Co_3O_4. [28-30] The bands in the frequency range of 1300-1600 cm^{-1} show the typical vibrations of the hemoglobin porphyrin macrocycles tied to MNPs surfaces.[31-34] The ν_4 oxidation state vibration marker band at 1371 cm^{-1} reveals that the irons of heme groups are mainly in the ferric state.[31] The ν_2 vibrational mode which is sensitive to the spin state of the iron atom is observed at 1585 cm^{-1}, indicating that the redox groups of the proteins are in a six-coordinated low spin configuration (6cLS).[34] Both methodologies (FT-IR, and Raman measurements) were generally in good agreement, supporting the validity of our assumption on preserved native protein structure after the synthetic process.

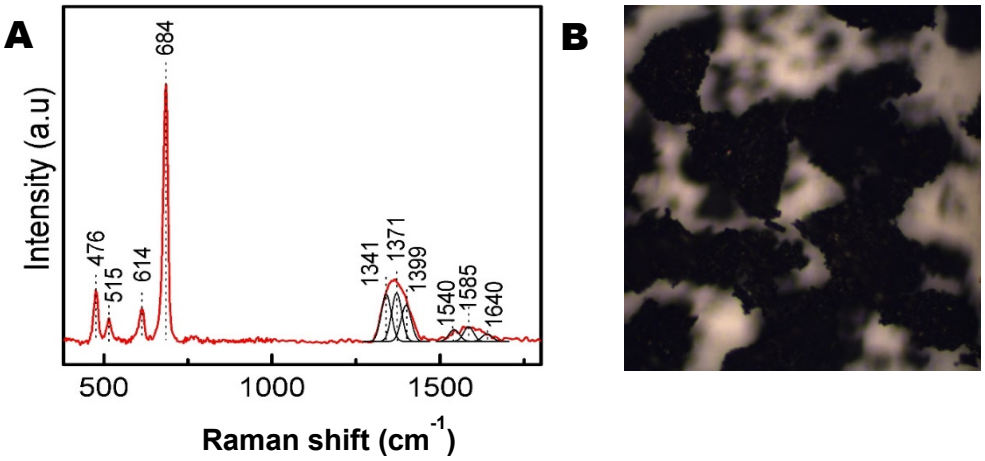

Fig. 3 (A) Raman spectrum. Excitation at λ=532nma and (B) Raman images of Hb-DA-Co_3O_4 nanoparticles.

The morphology of both parent MNPs and Hb-DA-Co_3O_4 nanomaterials was determined by TEM analysis. TEM micrographs depict a homogeneous distribution of the magnetic nanoparticles for both materials with a mean diameter of 10.1±0.2 nm. In the case of Hb-DA-Co_3O_4, the magnetic nanoparticles could be entrapped by the protein, with a significant tendency to form agglomerates that can be observed (Fig. 4), being also an evidence of the aggregation of Hb on the surface of the nanomaterials.

The dynamic light scattering data of the Hb-DA-Co_3O_4 conjugate (see Fig. 5a) revealed an appreciable degree of agglomeration with an average hydrodynamic size of 177 nm. After the protein functionalization, the zeta potential of DA-Co_3O_4 decreased from 4.9 mV to -1.8 mV (see Fig. 5b and S5, ESI†), which is in agreement with the zeta potential of the Hb in solution and confirms the successful anchorage of the protein on the MNP surfaces.[35,36]

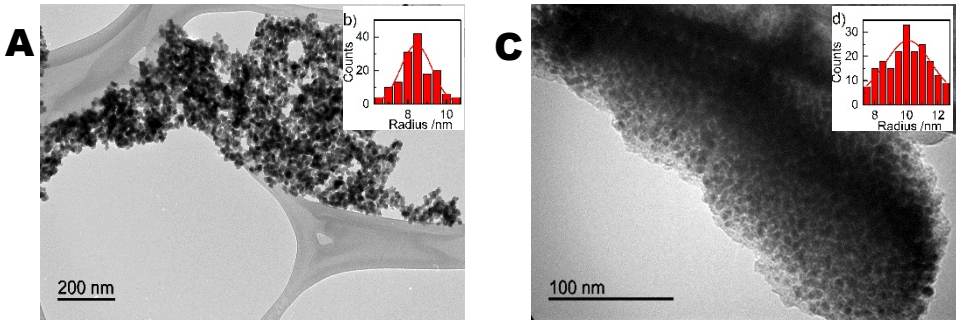

Fig. 4 TEM images of the (A) MNPs and (C) Hb-DA-Co_3O_4; particle distribution of (B) MNPs and (D) Hb-DA-Co_3O_4

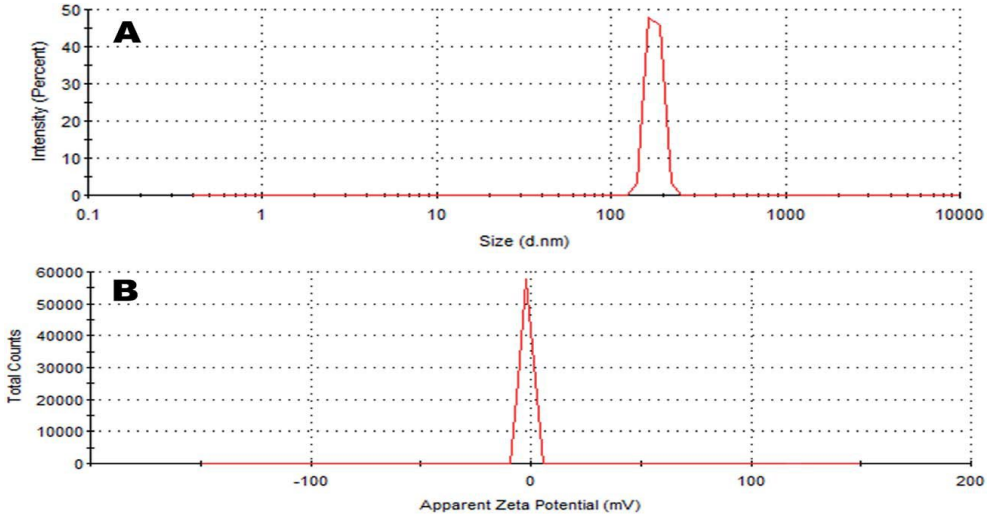

Fig. 5 (A) Dynamic scattering data and (B) zeta potential of the Hb-DA-Co_3O_4 nanobioconjugate.

Thermogravimetric analysis was performed to investigate the desorption-calcination of both materials: (A) MNPs and (B) Hb-DA-Co_3O_4 (Fig. 6). The first weight loss at 100 ºC in

both, MNPs and Hb-DA-Co_3O_4 (endothermic-TDA signal) can be correlated to the presence of water in the materials. From 220 ºC and 250 ºC for MNPs and Hb-DA-Co_3O_4 respectively, a progressive weight loss was observed, that can be assigned to the non-oxidative decomposition of organic species present in the materials. Interestingly, DTA experiments of Hb-DA-Co_3O_4 clearly exhibited two sharp endothermic bands at 270 and 320 ºC, corresponding to the decomposition of the protein in the material. Comparably, no bands could be observed in this range despite a similar TG mass loss profile. These findings also support the proposed presence of Hb on Hb-DA-Co_3O_4.

The magnetic susceptibilities measured for both MNPs and Hb-DA-Co_3O_4 resulted in similar values, with a slightly lower value for the bio-modified nanomaterial (Table 1). The observed loss could be both attributed to the protein loading after functionalisation as well to the functionalised material itself. In any case, without any considerable loss of magnetism after the synthetic process, both materials feature attractive properties for magnetic separation and manipulation in view of potential applications.

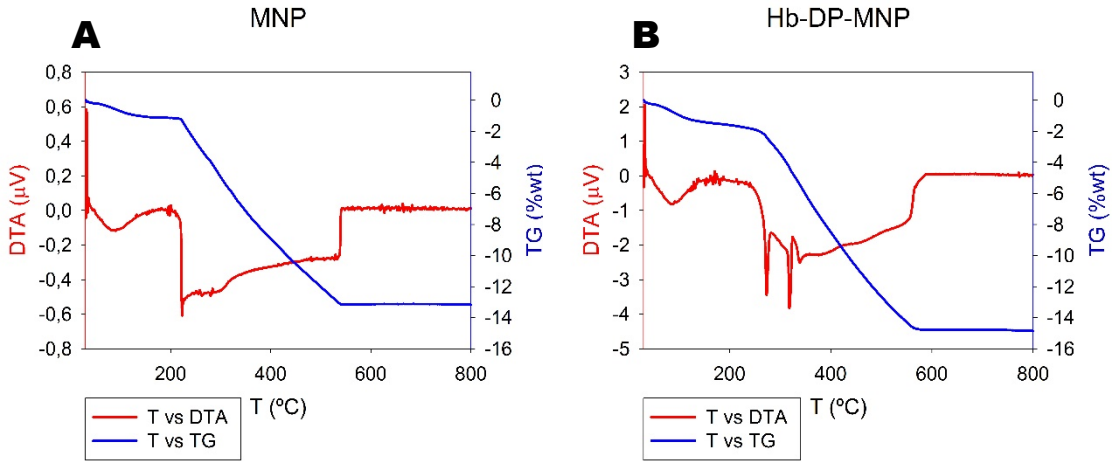

Fig. 6 ATG of the (A) MNPs and (B) Hb-DA-Co_3O_4

Table 1 Magnetic susceptibility of the Hb-DA-Co_3O_4 and MNPs

Material	Magnetic susceptibility (10^{-6} m^3Kg^{-1})
MNPs	370
Hb-DA-Co_3O_4	357

Electrochemical analysis

The cyclic voltammograms (CV) of (A) MNPs, (B) DA-Co_3O_4 and (C) Hb-DA-Co_3O_4 nanocomposites in 0.1M PBS at a scan rate of 100 mV/s are depicted in Fig. 7. No redox peaks were observed for MNPs and DA-Co_3O_4 as expected (Fig. 7a and b), indicating a non-electroactive behaviour of both nanostructured materials. Comparably, cyclic voltammograms of Hb-DA-Co_3O_4 nanocomposite (Fig. 7c) showed two well-defined redox peaks located at 0.007 V and -0.097 V vs Ag/AgCl respectively. These results can be associated with the Hb-heme Fe (III)/Fe (II) redox couple[37, 38] and suggest that a fraction of Hb immobilized on MNPs surface adopted an active electron transfer (ET) orientation. The cyclic voltammetry of Hb-DA-Co_3O_4 was consistent with a pseudocapacitance behavior where the charge and discharge processes are associated with oxidation and reduction peaks,[39, 40] whereas the voltammogram of MNPs displayed a rectangular shape, typical of a pure electrostatic capacitor.[41]

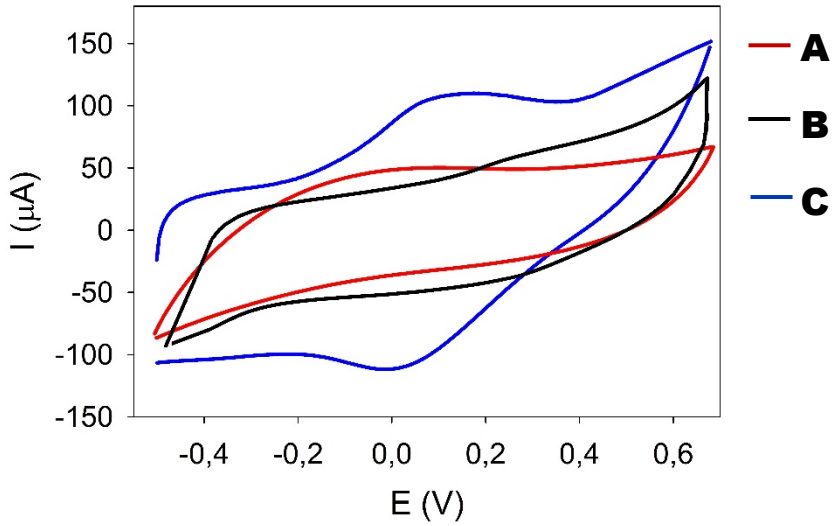

Fig. 7 Representative cyclic voltammograms of (A) MNPs, (B) DA-Co_3O_4 and (C) Hb-DA-Co_3O_4 nanocomposites at the scan rate of 100 mV/s in 0.1 M PBS pH=7.

The presence of pseudocapacitance in Hb-DA-Co_3O_4 was also evidenced in galvanostatic charge and discharge cycling profiles (Fig. 8). The nanocomposite clearly deviated from the triangular shape of an ideal capacitor in which the electrostatic charge is accumulated in the double layer of the electrolyte-electrode interface.[42] A significant hump in the charge branch of the cycles was observed, in agreement with the expected pseudocapacitance behaviour of redox molecules.[40, 42, 43] The galvanostatic measurements of DA–Co3O4 were also performed (see Fig. S6, ESI†). The obtained results indicate that the observed pseudocapacitance is due to the electron exchange at the redox groups of the electroactive hemoglobins immobilized on the DA-Co_3O_4 surfaces.

Hb-DA-Co_3O_4 possessed an average of specific capacitance of 115 F g^{-1}, certainly comparable with reported synthetic supercapacitors[44, 45] and with the specific capacitance reported for a supercapacitor based on c-type cytochromes using conductive nanostructured networks of living bacteria[24] (Table 2). Importantly, it should be pointed out that the specific capacitance of a Hb film has been reported to be 12.18 F g^{-1}, [46] which is 10 times lower that the one that we reported on this manuscript. This finding strongly confirmed the successful described

biosupercapacitor design. Although other nanomaterials provide higher capacitance values such as carbon nanotubes (CNTs) based networks materials (100-350 Fg^{-1}), metal oxide-carbon hybrid structures (200-700 Fg^{-1}) and conductive polymers (200-1000 Fg^{-1}),[47] they have several drawbacks based mainly in the high cost, tedious fabrication steps, and difficult scale up.

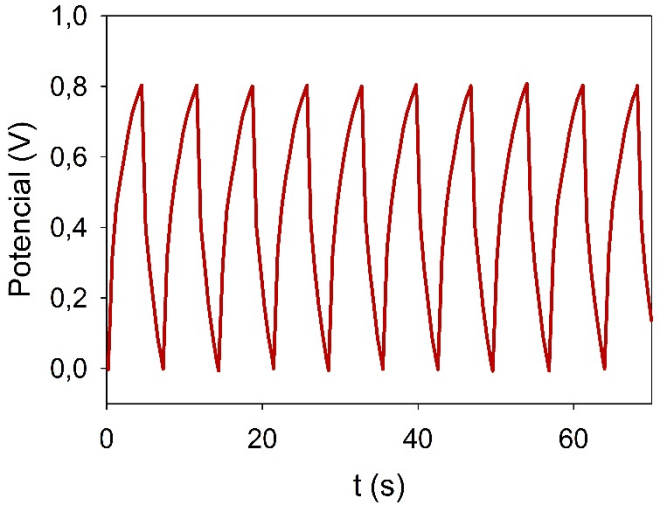

Fig. 8 Galvanostatic charge and discharge profile of Hb-DA-Co_3O_4, at a current density of 30Ag^{-1} in 0.5 M KOH aqueous solution.

Table 2 Specific capacitance of supercapacitors reported in the literature

Supercapacitor configuration	Intensity (mA)	Range of potential	Scan rate	Specific Capacitance (Fg^{-1}):	Reference
c-cytochromes on a microbial film	1	0-0.8	-	110[a]	24
Fe_3O_4 nanocrystals graphene composites	-	-	100mV/s	88[b]	41
graphene/MnO_2/ ACN asymmetric	-	-	1mV/s	113.5[b]	42
Hb-DA-Co_3O_4	0.5	0-0.8	30Ag^{-1}	115[a]	This work

[a] Specific capacitance obtained from galvanostatic curves and [b] Specific capacitance obtained from CV curves.

The specific capacitance of Hb-DA-Co_3O_4 as a function of the number of cycles has also been represented in Fig. 9. Approximately 94% (110 Fg^{-1}) of the initial specific capacitance (118 Fg^{-1}) could be measured after 1000 cycles, further demonstrating the high stability of the designed bio-nanocomposite and its excellent properties as a high-performance supercapacitor.

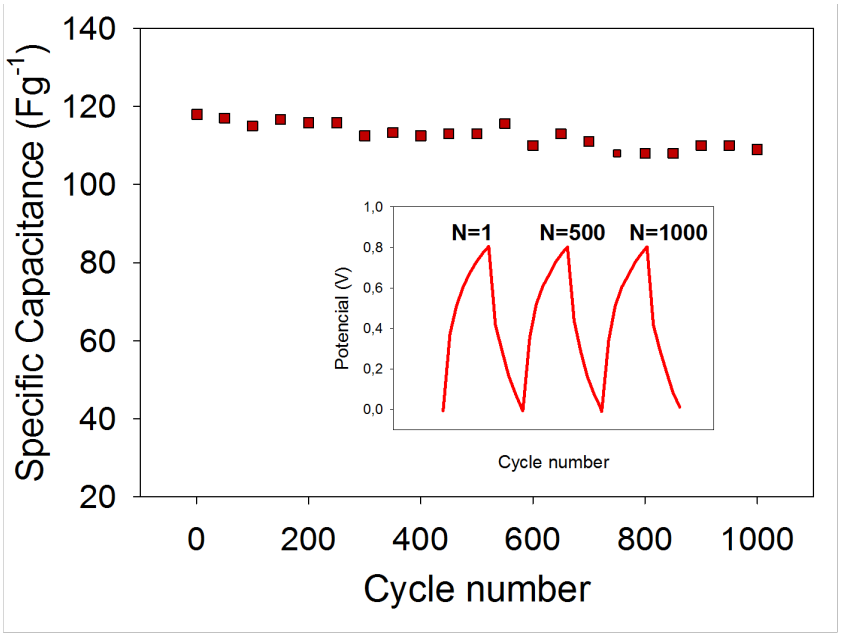

Fig. 9 Cycling behaviour of Hb-DA-Co_3O_4 nanocomposite at a current density of 30Ag^{-1} in 0.5 M KOH aqueous solution. Inset: different cycles of galvanostatic charge-discharge curves.

Conclusions

The design of a bio-inspired protein-functionalised magnetic nanomaterial containing horse hemoglobin, dopamine and a Co nanoferrite as support was successfully accomplished using a

mechanochemical approach. The proposed dry milling functionalisation was proven to be a simple, environmentally friendly and effective alternative methodoloy for the preparation of bio-modified materials for various applications. The incorporation of the protein on the surface of the Co-containing nanostructures was confirmed by XPS, DLS, FT-IR, Raman spectroscopy and TG/DTA, with fully preserved protein structure after the milling process. A novel and durable supercapacitor based could also be developed based on the obtained Hb-DA-Co_3O_4 nanocomposite. The assembled supercapacitor could be reversibly cycled in the voltage region of 0-0.8 V, exhibiting a maximum specific capacitance of 118 Fg^{-1} at a scan rate of 30 Ag^{-1}. Additionally, the supercapacitor device showed an excellent long cycle life along with 94% specific capacitance retained after 1000 cycles. We envisaged the proposed system and further modifications currently under investigation in our laboratories to pave the way to further developments of environmentally friendly and affordable bio-inspired energy storage devices for practical applications.

Acknowledgments

Rafael Luque gratefully acknowledges support from Consejeria de Ciencia e Innovacion, Junta de Andalucia for funding project P10-FQM-6711 as well as Spanish MINECO for funding Project CTQ2016-78289-P.

References

1. Y. Pan, X. W. Du, F. Zhao and B. Xu, *Chem. Soc. Rev.*, 2012, **41**, 2912.
2. S. Laurent, D. Forge, M. Port, A. Roch, C. Robic, L. V. Elst and R. N. Muller, *Chem. Rev.*, 2008, **108**, 2064.
3. K. Ulbrich, K. Hola, V. Subr, A. Bakandritsos, J. Tucek and R. Zboril, *Chem. Rev.*, 2016, **116**, 5338.
4. G. D. Liu, Y. H. Lin, V. Ostatna and J. Wang, *Chem. Commun.*, 2005, **27**, 3481.

5. D. Sarauli, C. Wettstein, K. Peters, B. Schulz, D. Fattakhova-Rohlfing and F. Lisdat, *ACS Catal.*, 2015, **5**, 2081.
6. P. R. Levison, S. E. Badger, J. Dennis, P. Hathi, M. J. Davies, I. J. Bruce and D. Schimkat, *J. of Chromatogr. A*, 1998, **816**, 107.
7. M. Uhlen, *Nature*, 1989, **340**, 733.
8. X. P. Jia, M. L. Xu, Y. Z. Wang, D. Ran, S. Yang and M. Zhang, *Analyst*, 2013, **138**, 651.
9. Z. W. Xia, Z. A. Lin, Y. Xiao, L. Wang, J. N. Zheng, H. H. Yang and G. N. Chen, *Biosensors & Bioelectronics*, 2013, **47**, 120.
10. T. J. Yoon, K. N. Yu, E. Kim, J. S. Kim, B. G. Kim, S. H. Yun, B. H. Sohn, M. H. Cho, J. K. Lee and S. B. Park, *Small*, 2006, **2**, 209.
11. R. Di Corato, N. C. Bigall, A. Ragusa, D. Dorfs, A. Genovese, R. Marotta, L. Manna and T. Pellegrino, *ACS Nano*, 2011, **5**, 1109.
12. J. Kim, H. S. Kim, N. Lee, T. Kim, H. Kim, T. Yu, I. C. Song, W. K. Moon and T. Hyeon, *Angew. Chem. Int. Ed.*, 2008, **47**, 8438.
13. O. Veiseh, J. W. Gunn and M. Q. Zhang, *Adv. Drug Delivery Rev.*, 2010, **62**, 284.
14. R. A. Bohara, N. D. Thorat and S. H. Pawar, *RSC Adv.*, 2016, **6**, 43989.
15. W. H. Zhou, C. H. Lu, X. C. Guo, F. R. Chen, H. H. Yang and X. R. Wang, *J. Mater. Chem.*, 2010, **20**, 880.
16. C. J. Xu, K. M. Xu, H. W. Gu, R. K. Zheng, H. Liu, X. X. Zhang, Z. H. Guo and B. Xu, *J. Am. Chem. Soc.*, 2004, **126**, 9938.
17. T. Rajh, L. X. Chen, K. Lukas, T. Liu, M. C. Thurnauer and D. M. Tiede, *J. Phys. Chem. B*, 2002, **106**, 10543.
18. T. Tsuzuki and P. G. McCormick, *J. Mater. Sci.*, 2004, **39**, 5143.
19. C. C. Koch, *Nanostructured Mater.*, 1993, **2**, 109.
20. J. Ding, Y. Shi, L. F. Chen, C. R. Deng, S. H. Fuh and Y. Li, *J. Magn. Magn. Mater.*, 2002, **247**, 249.
21. J. Ding, T. Tsuzuki and P. G. McCormick, *J. Mater. Sci.*, 1999, **34**, 5293.
22. M. L. Verma, C. J. Barrow, J. F. Kennedy and M. Puri, *Int. J. Biol. Macromol.*, 2012, **50**, 432.
23. H. Y. Gu, A. M. Yu and H. Y. Chen, *J. Electroanal. Chem.*, 2001, **516**, 119.
24. N. S. Malvankar, T. Mester, M. T. Tuominen and D. R. Lovley, *ChemPhysChem*, 2012, **13**, 463.
25. L. L. Zhang and X. S. Zhao, *Chem. Soc. Rev.*, 2009, **38**, 2520.

26. M. Ojeda, A. M. Balu, V. Barron, A. Pineda, A. G. Coleto, A. A. Romero and R. Luque, *J. Mater. Chem A*, 2014, **2**, 387.
27. K. Jiang, S. Sun, L. Zhang, Y. Lu, A. G. Wu, C. Z. Cai and H. W. Lin, *Angew. Chem., Int. Ed.*, 2015, **54**, 5360–5363.
28. Y. Lou, L. Wang, Y. H. Zhang, Z. Y. Zhao, Z. G. Zhang, G. Z. Lu and Y. Guo, *Catalysis Today*, 2011, **175**, 610.
29. Q. Liu, L. C. Wang, M. Chen, Y. Cao, H. Y. He and K. N. Fan, *Journal of Catalysis*, 2009, **263**, 104.
30. L. J. Dai, M. Liu, Y. Song, J. J. Liu and F. Wang, *Nano Energy*, 2016, **27**, 185.
31. T. G. Spiro, J. D. Stong and P. Stein, *J. Am. Chem. Soc.*, 1979, **101**, 2648.
32. M. Feng and H. Tachikawa, *J. Am. Chem. Soc.*, 2008, **130**, 7443.
33. B. R. Wood, M. Asghari-Khiavi, E. Bailo, D. McNaughton and V. Deckert, *Nano Lett.*, 2012, **12**, 1555.
34. G. Kalaivani, A. Sivanesan, A. Kannan, N. S. V. Narayanan, A. Kaminska and R. Sevvel, *Langmuir*, 2012, **28**, 14357.
35. M. Mahato, P. Pal, B. Tah, M. Ghosh and G. B. Talapatra, *Colloids Surf., B*, 2011, **88**, 141–149.
36. I. Sur, D. Cam, M. Kahraman, A. Baysal and M. Culha, *Nanotechnology*, 2010, **21**, 175104.
37. N. Zheng, X. Zhou, W. Y. Yang, X. J. Li and Z. B. Yuan, *Talanta*, 2009, **79**, 780.
38. L. S. Xuan Xu, Qiquin Seng, Xiadong Cao and Cheng Yao, *Electroanalysis*, 2016, **28**, 1.
39. Z. Gonzalez, B. Ferrari, A. J. Sanchez-Herencia, A. Caballero and J. Morales, *Electrochimica Acta*, 2016, **211**, 110.
40. Y. X. Xu, Z. Y. Lin, X. Q. Huang, Y. Wang, Y. Huang and X. F. Duan, *Adv. Mater.*, 2013, **25**, 5779.
41. S. Roldan, Z. Gonzalez, C. Blanco, M. Granda, R. Menendez and R. Santamaria, *Electrochimica Acta*, 2011, **56**, 3401.
42. S. Roldan, C. Blanco, M. Granda, R. Menendez and R. Santamaria, *Angew. Chem. Int. Ed.*, 2011, **50**, 1699.
43. B. E. Conway, *Electrochemical Supercapacitors:Scientific Fundamentals and Technological Applications*, Kluwer/Plenum, New York, **1999**.

44. B. J. Li, H. Q. Cao, J. Shao, M. Z. Qu and J. H. Warner, *J. Mater. Chem.*, 2011, **21**, 5069.
45. Z. J. Fan, J. Yan, T. Wei, L. J. Zhi, G. Q. Ning, T. Y. Li and F. Wei, *Adv. Funct. Mater.*, 2011, **21**, 2366.
46. M. Khairy and S. A. El-Sa□y, *J. Energy Chem*., 2015, **24**, 31–38.
47. H. Jiang, P. S. Lee and C. Z. Li, *Energy & Environmental Science*, 2013, **6**, 41.